Electronic Supplementary Information

γ-Fe_2O_3 Nanoparticle Surface Controls PtFe Nanoparticle Growth and Catalytic Properties

Gregory Gumina, Rosemary Easterday, Andrey G. Malyutin, Angela M. Budgin, Barry D. Stein, Linda Zh. Nikoshvili, Valentina G. Matveeva, Esther M. Sulman, David Gene Morgan, Lyudmila M. Bronstein**

1. Experimental Procedures

1.1. Materials

$FeCl_3 \cdot 6H_2O$ (98%), octadecane (99%), eicosane (99%), dioctyl ether (99%), 1,2-hexadecane diol (90%), oleylamine (OAm, 70%), oleic acid (OA, 90%), platinum (II) acetylacetonate (97%, $Pt(acac)_2$), toluene (99.8%) and methyl-3-buten-2-ol (≥98%) were purchased from Sigma-Aldrich and used as received. Hexanes (98.5%) and ethanol (95%) were purchased from EMD Chemicals and used as received. Acetone (99.5%) and chloroform (99.8%) were purchased from MACRON Chemicals and also used without purification.

1.2. Synthetic Procedures

1.2.1. Syntheses of FeO/Fe_3O_4 Iron Oxide Nanoparticles

The synthesis of iron oleate was carried out using a published procedure.[1] The FeO/Fe_3O_4 NPs were synthesized in octadecane or eicosane as a solvent according to procedures published elsewhere.[2,3] The NPs were precipitated from the solid iron oxide reaction solutions on as needed basis. The typical iron oxide NPs formed in octadecane are shown in Figure S1a.

1.2.2. Oxidation of FeO/Fe_3O_4 Nanoparticles to γ-Fe_2O_3 Nanoparticles

Reaction solutions of as-prepared NPs were melted to transfer a few milliliters to a three-neck flask equipped with a reflux condenser and a stir bar. Then the solution was heated to 200 °C and left to stir for 2 hours under air.[3] Purification of these NPs is similar to that described elsewhere.[2,3] Oxidized NPs are shown in Figure S1b. These data clearly show that the NP morphology remains unchanged after oxidation. Inset in b shows that NPs are spherical.

The structure of NPs before and after oxidation was determined by X-ray powder diffraction as FeO/Fe_3O_4 and γ-Fe_2O_3, respectively, as is reported in our preceding papers.[2,3]

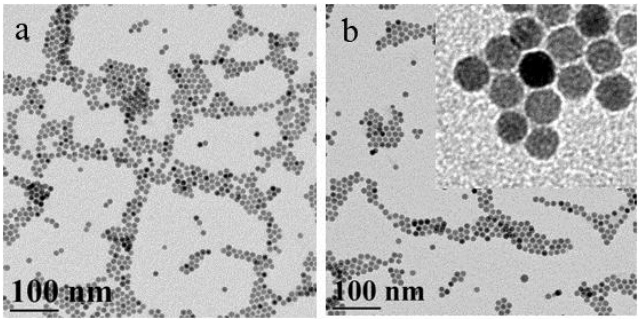

Figure S1. As-synthesized FeO/Fe3O4 NPs with a diameter of 11.4 nm and a standard deviation of 7.9% (a) and γ-Fe2O3 NPs with a diameter of 11.7 nm and a standard deviation of 8.6% (b).

The characteristics of the γ-Fe_2O_3 NPs used in this work are presented in Table 1. The amount of OA on the nanoparticle surface was determined via weight loss obtained from the thermal gravimetric analysis (TGA) data. The data for the majority of samples are presented in Table 1.

1.3. Characterization

Electron-lucent NP specimens for TEM were prepared by placing a drop of dilute solution onto a carbon-coated Cu grid. Images were acquired at an accelerating voltage of 80 kV on a JEOL

JEM1010 transmission electron microscope. Images were analyzed with the National Institute of Health developed image-processing package ImageJ to estimate NP diameters. Between

TEM (HRTEM) images and energy dispersive X-ray spectra (EDS) were acquired at accelerating voltage 300 kV on a JEOL 3200FS transmission electron microscope equipped with an Oxford Instruments INCA EDS system. The same TEM grids were used for both analyses.

X-ray diffraction (XRD) patterns were collected on a Scintag theta-theta powder diffractometer with a Cu $K_{\square}$ source (0.154 nm).

TGA was performed on TGAQ5000 IR manufactured by TA Instruments. The NP solution was evaporated into a 100 µL platinum pan and dried. The experiments were carried upon heating to 700 °C at the rate of 10.0 ^{o}C/min.

1.4. Catalytic tests

Catalytic experiments were carried out in a 60 mL iso-thermal glass batch reactor installed in a shaker and connected to a gasometrical burette. The reactor was equipped with two inlets: one for catalyst, solvent, and substrate, and the other for hydrogen feed. The total volume of liquid phase was 30 mL. Hydrogen consumption was controlled by a gasometrical burette. Reaction conditions were the following: toluene as a solvent, an ambient hydrogen pressure, a temperature of 95 °C, a stirring rate at 850 shakings per minute, a substrate-to-Pt molar ratio of 3035.

Samples for analysis were taken depending on the hydrogen consumption and analyzed via GC using Kristallux-4000 chromatograph with FID and Agilent HP-1MS capillary column (30 m x 0.25 mm i.d., 0.25 µm film thickness).

2. Pt, PtFe, and γ-Fe_2O_3 Nanoparticles

XRD diffraction profile presented in Figure S2 (ESI) shows typical reflections for the face-centered cubic (*fcc*) Pt structure (PDF 4-802), in agreement with the results published by others for PtFe NPs.[4] When PtFe alloy is formed, diffraction peaks are shifted toward higher 2θ values as compared to those of Pt.[5] The shift in a peak position shows the lattice contraction due to the partial substitution of Pt by Fe atoms in the Pt *fcc* structure and demonstrates the presence of a PtFe alloyed phase. In our case, the (220) diffraction peak, for example, is shifted to 69°, while for pure Pt, the position of this peak is at 67.5°.[6] Using the Scherrer formula for the line broadening of the (110) peak, we obtained the nanocrystal size of 2.8 nm which is consistent with the TEM data.

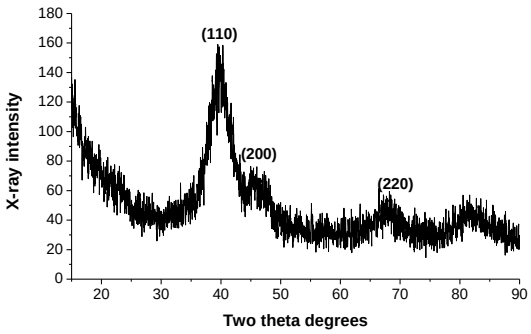

Figure S2. XRD profile of Pt_3Fe NPs.

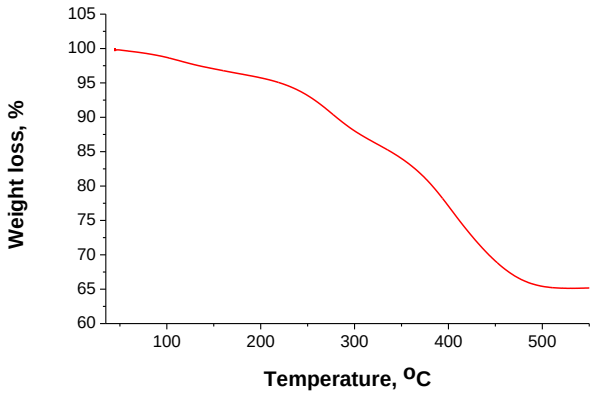

Figure S3. TGA curve of the Pt_3Fe NPs.

We determined the amount of capping molecules (OAm and OA) on the Pt_3Fe NP surface using TGA (Fig. S3). For calculation of the amount of molecules on the NP surface, the PtFe density is needed. However, because the PtFe density is unknown, we calculated the average density taking into account the density of three Pt atoms and one Fe and dividing by four, resulting in the density of 18.056 g/cm^3. The total weight loss upon heating the sample to 550 °C is 35 wt.%. The amount of oleic acid and oleylamine molecules was calculated taking into account 35% weight loss. The amount of NPs was calculated from the remainder of the sample (65 wt.%).

This allowed us to calculate the total amount of OAm and OA molecules on the NP surface and the surface area under one ligand. The latter value of 0.24 nm^2 is comparable with that of thiols (0.156 nm^2) adsorbed on the gold NP surface.[7]

When the $Pt(acac)_2$ decomposition is carried out in similar conditions but in the *absence* of maghemite NPs, the purely Pt NPs formed are mainly aggregated (Fig. S4a, ESI). The NPs remaining in solution have a broad particle size distribution. The STEM EDS map confirms that they consist of pure Pt (Fig. S4b, c).

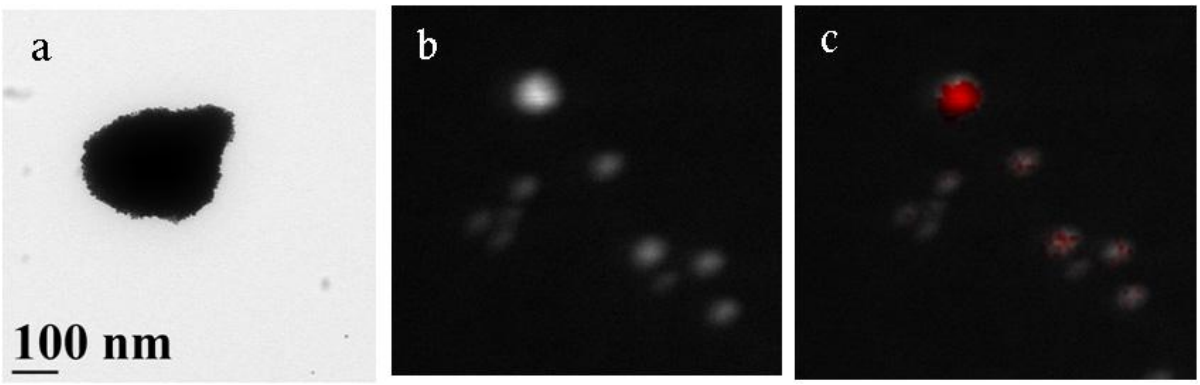

Figure S4. (a) TEM image of the aggregate of Pt NPs. (b) Dark field STEM image of Pt NPs remaining in solution. (c) EDS STEM Pt map overlaid on the image presented in (b).

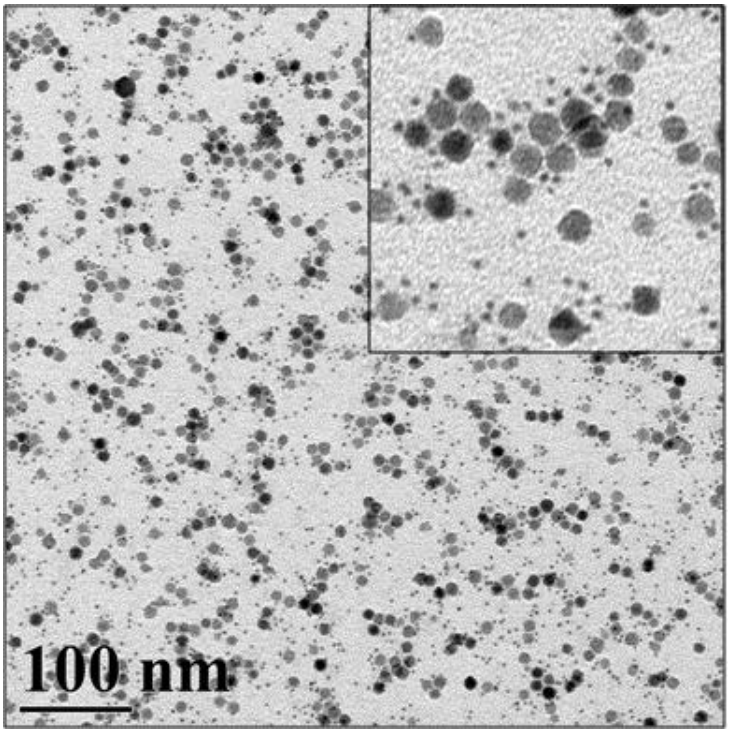

Figure S5. TEM image of PtFe (smaller) and γ-Fe_2O_3 (larger) NPs obtained in the synthesis with a double amount of OA and OAm (Pt/γ-Fe_2O_3-2). Inset (a higher magnification image) shows that the remaining γ-Fe_2O_3 are not perfectly spherical anymore.

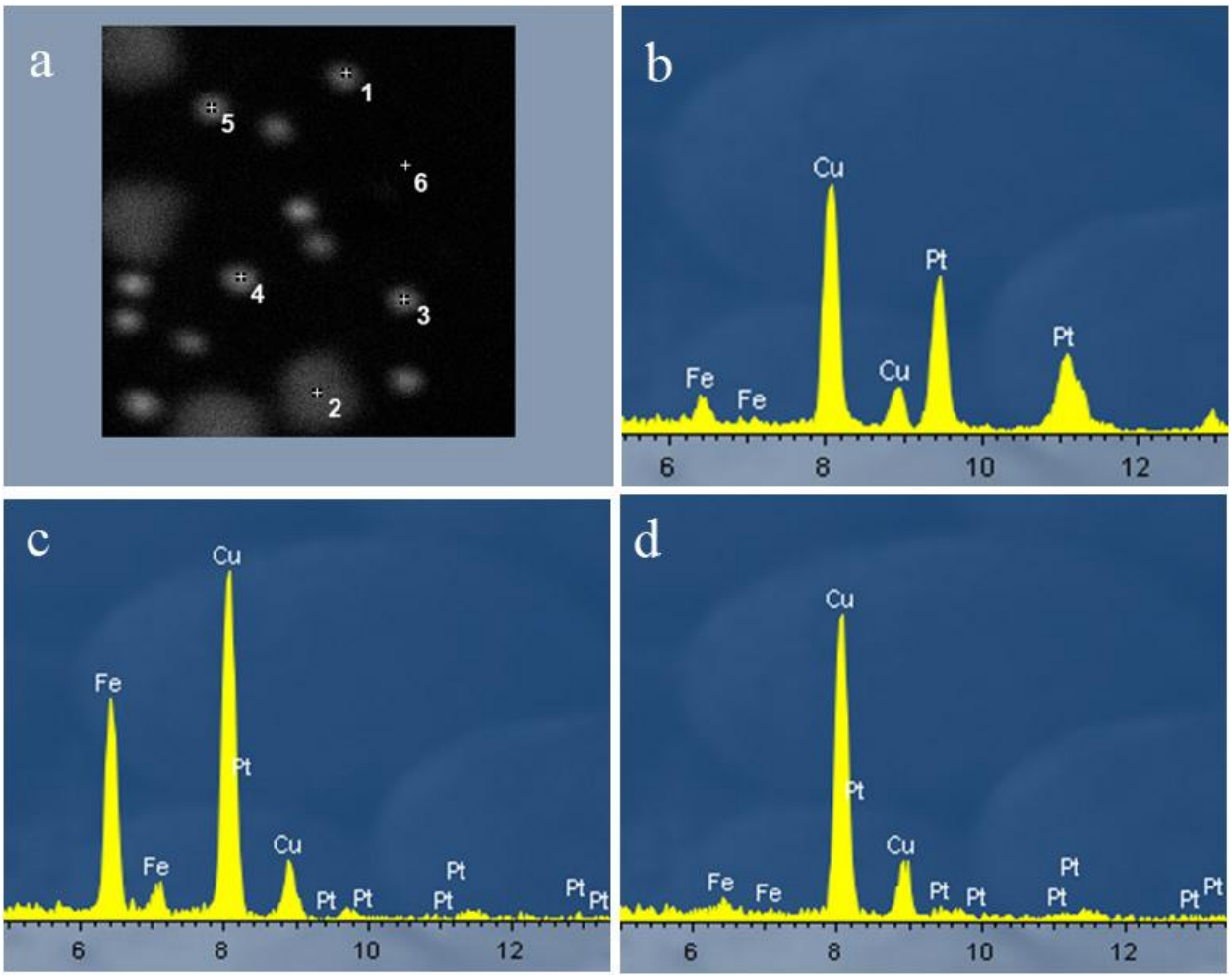

Figure S6. Annotated dark-field STEM image (a) and the EDS spectra for NPs in the positions 1 (b) and 2 (c) and for the background in position 6 (d) for the sample prepared with the double amount of surfactants and shown in Figure S5.

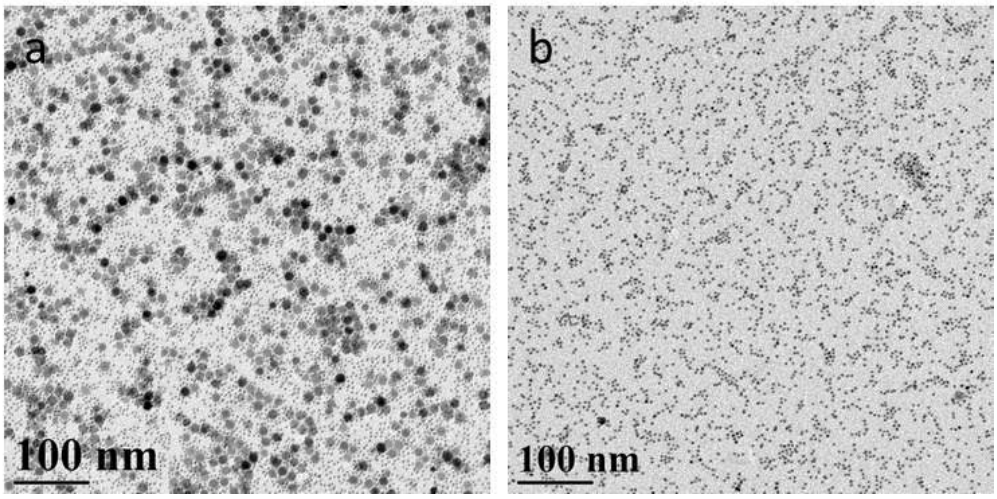

Figure S7. TEM images of Pt/γ-Fe2O3-6 (a) and Pt/γ-Fe2O3-5 (b) using OC-12.4 NPs as-synthesized and OC-12.7 oxidized, respectively.

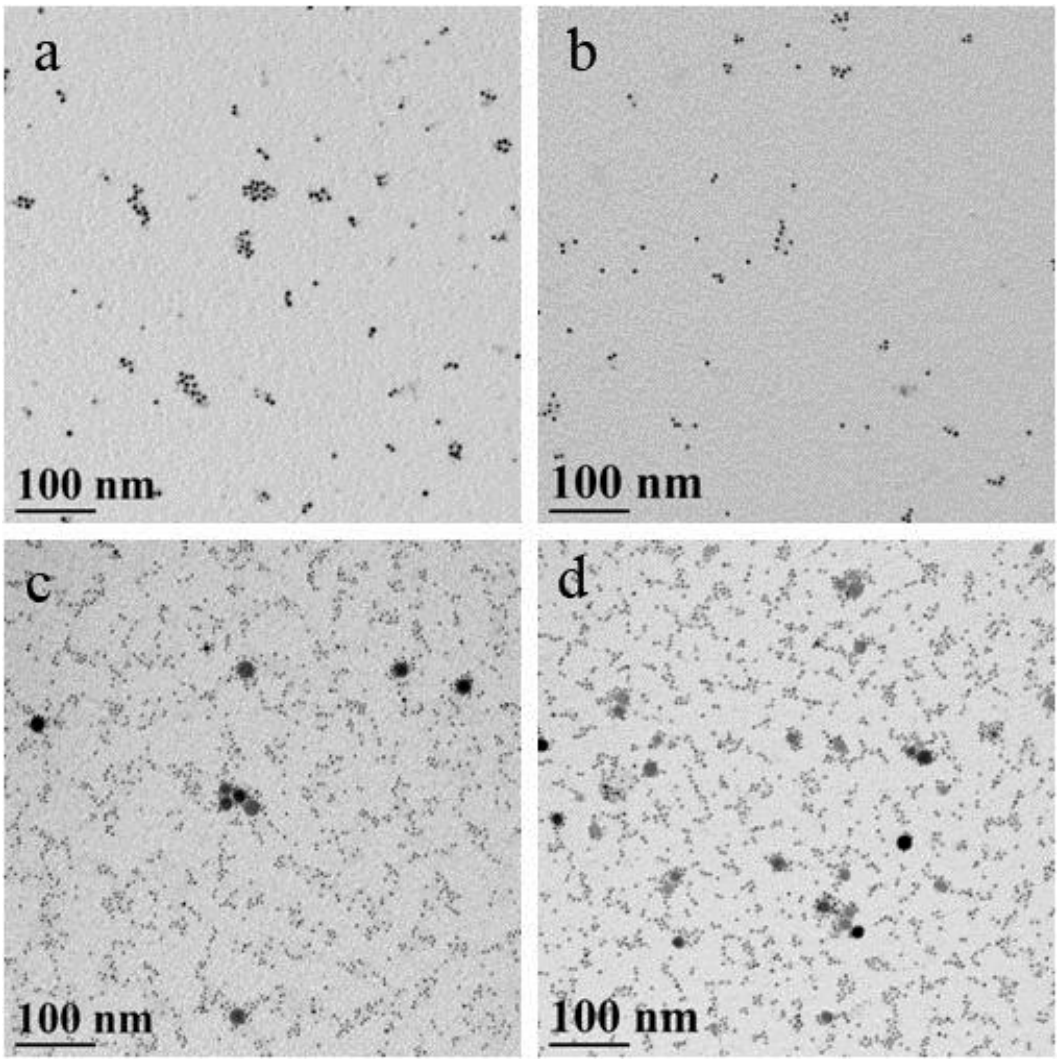

Figure S8. TEM images of the samples Pt/γ-Fe2O3-10 (a), Pt/γ-Fe2O3-11 (b), Pt/γ-Fe2O3-12 (c), and Pt/γ-Fe2O3-13 (d) prepared in the presence of 20.9 nm and 21.3 nm γ-Fe_2O_3 NPs at different amounts of surfactants (see Table 1 for conditions).

Figure S9. Photograph of magnetic separation of the Pt/γ-Fe_2O_3-2 catalyst after hydrogenation.

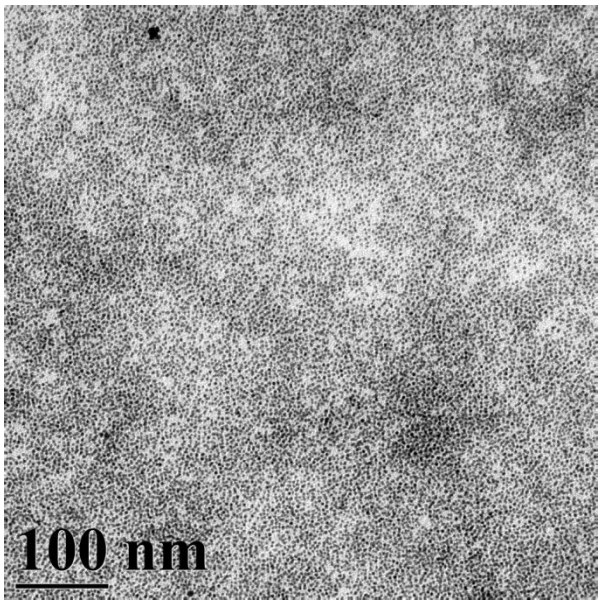

Figure S10. TEM image of the Pt_3Fe NPs evaporated from the toluene solution on a water surface.

References

(1) Park, J.; An, K.; Hwang, Y.; Park, J.-G.; Noh, H.-J.; Kim, J.-Y.; Park, J.-H.; Hwang, N.-M.; Hyeon, T. *Nature Mater.* **2004**, *3*, 891.

(2) Bronstein, L. M.; Huang, X.; Retrum, J.; Schmucker, A.; Pink, M.; Stein, B. D.; Dragnea, B. *Chem. Mater*. **2007**, *19*, 3624.

(3) Bronstein, L. M.; Atkinson, J. E.; Malyutin, A. G.; Kidwai, F.; Stein, B. D.; Morgan, D. G.; Perry, J. M.; Karty, J. A. *Langmuir* **2011**, *27*, 3044.

(4) Malheiro, A. R.; Varanda, L. C.; Perez, J.; Villullas, H. M. *Langmuir* **2007**, *23*, 11015.

(5) Malheiro, A. R.; Perez, J.; Santiago, E. I.; Villullas, H. M. *J. Phys. Chem. C* **2010**, *114*, 20267.

(6) Boennemann, H.; Nagabhushana, K. S.; Richards, R. M.; From Nanoparticles and Catalysis (2008) In *Nanopartciles and Catlysis*; Astruc, D., Ed.; Wiley-VCH Verlag GmbH & Co. KGaA: Weinheim, Germany, 2008, p 49.

(7) Kimura, K.; Takashima, S.; Ohshima, H. *J. Phys. Chem. B* **2002**, *106*, 7260.